Free Radical Biology and Medicine 162 (2021) 298–308

Contents lists available at ScienceDirect

Free Radical Biology and Medicine

journal homepage: www.elsevier.com/locate/freeradbiomed

Original article

Xanthine oxidase inhibition attenuates doxorubicin-induced cardiotoxicity in mice

Yoshiro Tanaka, Tomohisa Nagoshi *, Akira Yoshii, Yuhei Oi, Hirotake Takahashi, Haruka Kimura, Keiichi Ito, Yusuke Kashiwagi, Toshikazu D. Tanaka, Michihiro Yoshimura

Division of Cardiology, Department of Internal Medicine, The Jikei University School of Medicine, Japan

ARTICLE INFO

Keywords:
Xanthine oxidase
Doxorubicin
Uric acid
Reactive oxygen species
Purine metabolism

ABSTRACT

Accumulating evidence suggests that high serum uric acid (UA) is associated with left ventricular (LV) dysfunction. Although xanthine oxidase (XO) activation is a critical regulatory mechanism of the terminal step in ATP and purine degradation, the pathophysiological role of cardiac tissue XO in LV dysfunction remains unclear. We herein investigated the role and functional significance of tissue XO activity in doxorubicin-induced cardiotoxicity. Either doxorubicin (10 mg/kg) or vehicle was intraperitonially administered in a single injection to mice. Mice were treated with or without oral XO-inhibitors (febuxostat 3 mg/kg/day or topiroxostat 5 mg/kg/day) for 8 days starting 24 h before doxorubicin injection. Cardiac tissue XO activity measured by a highly sensitive assay with liquid chromatography/mass spectrometry and cardiac UA content were significantly increased in doxorubicin-treated mice at day 7 and dramatically reduced by XO-inhibitors. Accordingly, XO-inhibitors substantially improved LV ejection fraction (assessed by echocardiography) and LV developed pressure (assessed by ex vivo Langendorff heart perfusion) impaired by doxorubicin administration. This was associated with an increase in XO-derived hydrogen peroxide production with concomitant upregulation of apoptotic and ferroptotic pathways, all of which were reduced by XO-inhibitors. Furthermore, metabolome analyses revealed enhanced purine metabolism in doxorubicin-treated hearts, and XO-inhibitors suppressed the serial metabolic reaction of hypoxanthine–xanthine–UA, the paths of ATP and purine degradation. In summary, doxorubicin administration induces cardiac tissue XO activation associated with impaired LV function. XO-inhibitors attenuate doxorubicin-induced cardiotoxicity through inhibition of XO-derived oxidative stress and cell death signals as well as the maintenance of cardiac energy metabolism associated with modulation of the purine metabolic pathway.

1. Introduction

Increasing evidence indicates that elevated serum uric acid (UA) levels are an independent marker of cardiac dysfunction and oxidative stress in several cardiovascular diseases [1–4]. Indeed, high serum UA levels predict an increase in morbidity and mortality in patients with heart failure [5,6]. We recently reported a close link between high UA levels and left ventricular (LV) dysfunction in patients with cardiovascular diseases, including ischemic heart diseases [7].

UA is a final oxidation product of the metabolic breakdown of purine nucleotides [8]. Xanthine oxidoreductase (XOR) reaction is the critical rate-limiting step in adenosine triphosphate (ATP) and purine degradation. Mammalian XOR exists in two inter-convertible forms: xanthine dehydrogenase (XDH), the native form of the enzyme in the tissues under normal condition, can be converted reversibly to xanthine oxidase (XO) by oxidation of cysteine residues or irreversibly by limited proteolysis under pathological conditions [9–12]. In the process of catalyzing the oxidation of hypoxanthine to xanthine and xanthine to UA, XDH uses the oxidized form of nicotinamide adenine dinucleotide (NAD^+) as an electron acceptor and reduces it to nicotinamide adenine dinucleotide (NADH), whereas XO uses molecular oxygen as an electron acceptor and reduces it to superoxide anions (O_2^-) and hydrogen peroxide (H_2O_2), which are important sources of reactive oxygen species (ROS) [13–16], leading to cardiac dysfunction through the inhibition of ATP synthesis in the heart [17]. It is therefore possible that the cardiac tissue UA level might increase in the failing heart as a result of the activation of cardiac XO.

While previous studies have shown the enhanced cardiac XO activity in various experimental models of LV dysfunction [18–23], the

* Corresponding author. 3-25-8, Nishi-Shinbashi, Minato-ku, Tokyo, 105-8461, Japan .
E-mail address: tnagoshi@jikei.ac.jp (T. Nagoshi).

https://doi.org/10.1016/j.freeradbiomed.2020.10.303
Received 22 June 2020; Received in revised form 15 October 2020; Accepted 20 October 2020
Available online 24 October 2020

List of abbreviations

ADP	adenosine diphosphate
AMP	adenosine monophosphate
ATP	adenosine triphosphate
Dox	doxorubicin
GPX4	glutathione peroxidase 4
G6P	glucose-6-phosphate
Feb	febuxostat
FS	fractional shortening
HPRT	hypoxanthine guanine phosphoribosyltransferase
LC/MS	liquid chromatography-mass spectrometry
LVDP	left ventricular developed pressure
LVEF	left ventricular ejection fraction
PPP	pentose phosphate pathway
PRPP	phosphoribosyl diphosphate
ROS	reactive oxygen species
RPP	rate pressure product
Topi	topiroxostat
R5P	ribose 5-phosphate
UA	uric acid
XO	xanthine oxidase

expression and enzymatic activity of XO in the heart is generally low compared to other organs, such as small intestine, liver, lung, and adipose tissues [8,13]. In fact, cardiac XO is not significantly activated in some experimental models of myocardial injury, although XO-inhibitors still show substantial cardioprotective effects [24–26]. Therefore, the pathophysiological role and functional consequence of tissue XO activation in the failing heart remain incompletely understood.

Doxorubicin (Dox), an anthracycline antibiotic also known as adriamycin, is a chemotherapeutic agent widely used for the treatment of a wide range of malignancies. However, the clinical use of Dox is limited by its serious drawback of cardiotoxicity. While the mechanisms underlying Dox-induced cardiotoxicity have been studied extensively [27–31], the involvement and pathophysiological significance of cardiac tissue XO activation in Dox-induced cardiac dysfunction remain to be fully elucidated.

To better understand the role and the functional significance of XO activity in Dox-induced cardiotoxicity, we investigated whether cardiac XO was activated in Dox-treated mice and whether XO-inhibitors ameliorated LV function by inhibiting ROS and cell death signals as well as by modifying cardiac purine metabolism.

2. Materials and methods

2.1. Animal models

The study design is shown in Fig. 1A. All animal procedures conformed to the National Institutes of Health Guide for the Care and Use of Laboratory Animals and were approved by the Animal Research Committee at the Jikei University School of Medicine (2016-038C6). Male ICR mice at 10–12 weeks of age were fed normal chow (CE-2; CLEA Japan, Tokyo, Japan) mixed with or without XO-inhibitors; either febuxostat (Feb, 3 mg/kg/day, SML 1285; Sigma-Aldrich, Tokyo, Japan) or topiroxostat (Topi, 5 mg/kg/day, CS2033; Chemscene, Monmouth Junction, NJ, USA), for 8 days. One day after the initiation of the treatment with or without XO-inhibitors, either Dox (10 mg/kg, D1515; Sigma) dissolved in saline or an equal volume of saline was administered intraperitoneally. Mice were randomly assigned to six groups: control group, Feb-treated group, Topi-treated group, Dox-treated group, Dox-treated group treated with Feb, and Dox-treated group treated with Topi. As the dietary intake was decreased during the protocol in Dox-treated mice (Supplementary Fig. S1), the concentration of Feb and Topi mixed into the chow was adjusted accordingly in the Dox-treated

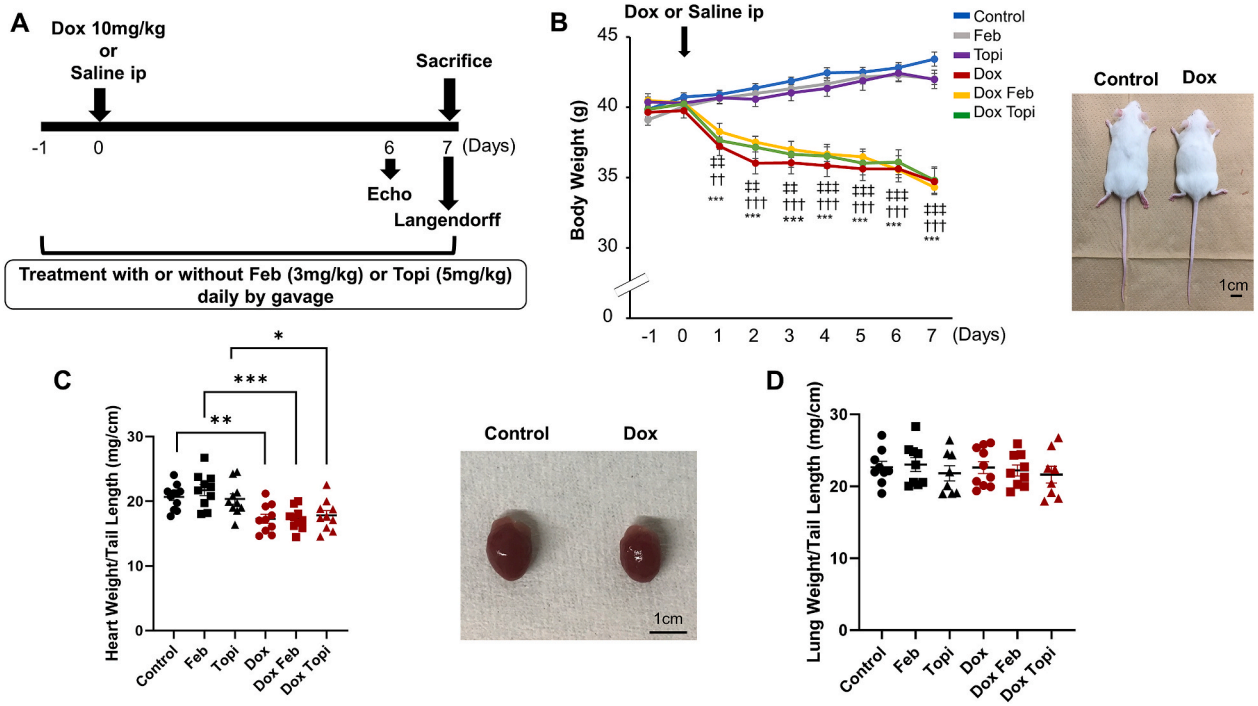

Fig. 1. The effects of Dox on the body and heart weights. (A) A schematic diagram of the experimental protocol. (B) Body weight changes during the protocol (Control, n = 11; Feb, n = 11; Topi, n = 9; Dox, n = 12; Dox + Feb, n = 11; Dox + Topi, n = 11). Heart weight (C) and lung weight (D) at 7 days after Dox administration with or without xanthine oxidase (XO) inhibitors treatment ([Heart weight] Control, n = 11; Feb, n = 10; Topi, n = 10; Dox, n = 10; Dox + Feb, n = 10; Dox + Topi, n = 10; [Lung weight] Control, n = 9; Feb, n = 9; Topi, n = 8; Dox, n = 10; Dox + Feb, n = 9; Dox + Topi, n = 8). Data are mean ± SEM. ***P < 0.001 and **P < 0.01, Dox vs. Control; †††P < 0.001 and ††P < 0.01, Dox + Feb vs. Feb; ‡‡‡P < 0.001, ‡‡P < 0.01 and ‡P < 0.05, Dox + Topi vs. Topi.

group in order to equalize the dosage amount of these drugs between groups.

2.2. XOR activities measurement

The XO activities in various tissues, including the heart, were measured using the horseradish peroxidase-linked Amplex Red fluorescence assay kit (Molecular Probes, Invitrogen Detection Technologies) [32], according to the manufacturer's protocol. In brief, tissues were homogenized in T-PER Tissue Protein Extraction (Thermo Fisher Scientific, USA) followed by centrifugation (14,000 g, 10 min, 4 °C). The resulting supernatant was added to a working solution containing Amplex Red reagent (100 μM), xanthine (0.2 mM), and horseradish peroxidase type (0.4 U/ml), incubated at 37 °C for 30 min, and the H_2O_2 production was measured. Fluorescence readings were made in duplicate in a 96-well plate at Ex/Em = 540/590 nm. The XO activity was corrected by the protein concentration of the supernatant measured by a Bradford assay.

Cardiac tissue XOR (XDH-plus-XO) and XO activities were also measured using liquid chromatography-mass spectrometry (LC/MS) at day 7 after Dox administration (Fig. 1A). Mice hearts at day 7 were snap-frozen in liquid nitrogen and stored at −80 °C prior to the analysis. Each frozen heart was minced with scissors in 4 vol of ice-cold 0.1 M phosphate-buffered saline (PBS; pH 7.5) containing 10 mM dithiothreitol, 0.5 mM EDTA-2Na, and protease inhibitor cocktail, and then it was homogenized with a Teflon pestle. Dithiothreitol was added in order to inhibit the oxidation of two critical cysteine residues of XDH and the resultant reversible conversion to XO during the experimental process, followed by gel filtration to remove excess dithiothreitol [9,11]. Homogenates were centrifuged at 20,000 g for 20 min at 4 °C to obtain the supernatant as the cytosolic fraction. The XOR and XO activities were measured using the method reported by Murase et al. [33] with some modifications. The cytosol was passed through a Sephadex G-25 column equilibrated with 20 mM Tris–HCl, 150 mM NaCl buffer (Tris–buffered saline [TBS]; pH 8.5) to remove any small molecules. At the initiation of the enzyme reaction, 25 μL of cytosol was added to TBS containing a final concentration of 400 μM [$^{13}C_2$,$^{15}N_2$]-xanthine and 7.98 μM oxonate (and 500 μM of NAD^+ for XOR activity measurement) with an adjusted total volume of 250 μL. After incubation for 5 min at 37 °C, 10-μL aliquots of the reaction mixture and 190 μL of TBS (20-fold dilution) were added to 300 μL of ice-cold acetonitrile with 100 μL methanol containing 4 μM [$^{13}C_3$,$^{15}N_3$]-uric acid (UA) as the internal standard in order to stop the reaction. After the sample was centrifuged at 20,000 g for 10 min at 4 °C, the supernatant was filtered with an ultrafiltration membrane. The [$^{13}C_2$,$^{15}N_2$]-UA was quantitated using an LC (Nexera X2; Shimadzu, Kyoto, Japan)-triple quadrupole mass spectrometer (Triple Quad 4500; SCIEX, Framingham, MA, USA). The cytosolic protein concentration was determined using the BCA protein assay kit (Takara Bio, Shiga, Japan). The XOR and XO activities were expressed as [$^{13}C_2$,$^{15}N_2$]-UA nmol/5 min/mg protein. The XDH activity was calculated by subtracting XO activity from XOR activity.

2.3. Echocardiography

The mice at day 6 were lightly anesthetized with 0.5%–1.0% isoflurane to maintain their heart rate between 500 and 600 bpm and placed in a supine position on a heating pad to preserve their body temperature. Echocardiography was performed using a high-resolution Vevo 3100 system (VisualSonics) equipped with a high-frequency ultrasound probe. The 2D M-mode was obtained at the level of the papillary muscle, and end diastolic thickness of intraventricular septum (IVSd), left ventricular end-diastolic dimension (LVDd), left ventricular posterior wall thickness (LVPWd), and left ventricular end systolic dimension (LVDs) were measured. The fractional shortening (FS) and ejection fraction (EF) were calculated using the Vevo 3100 software program (VisualSonics). All measurements were obtained in triplicate and averaged.

2.4. Experiments in langendorff hearts

At day 7, the mice were heparinized (1000 IU/kg, intraperitoneally [i.p.]) and anesthetized (pentobarbital, 60 mg/kg, i. p.) in order to eliminate suffering. The heart was then rapidly excised, and the aorta was cannulated onto a Langendorff apparatus, followed by retrograde-perfusion at a constant pressure (80 mmHg) with modified Krebs-Henseleit buffer (11 mM glucose, 118 mM NaCl, 4.7 mM KCl, 2.0 mM CaCl2, 1.2 mM MgSO4, 1.2 mM KH2PO4, 25 mM NaHCO3, and 0.5 mM EDTA), as previously described [34–36]. After stabilization by 10-min perfusion, the cardiac hemodynamics were measured using a water-filled balloon catheter introduced into the left ventricle.

2.5. Immunoblotting

Immunoblotting was performed as previously described [35,36] with mouse monoclonal anti-XO (1:200, #sc-398,548; Santa Cruz Biotechnology, CA, USA); rabbit monoclonal anti-Bcl-2 (1:500, #3498; Cell Signaling Technology, Tokyo, Japan), anti-cleaved-caspase3; (1:500, #9661; Cell Signaling Technology, Tokyo, Japan), anti-GPX4 (1:20,000, #ab125066; Abcam, Tokyo, Japan), and anti-GAPDH (1:5000, #2118; Cell Signaling Technology, Tokyo, Japan); or mouse polyclonal anti-Bax (1:1000, #2772; Cell Signaling Technology, Tokyo, Japan) and anti-caspase-3 (1:1000, #9662; Cell Signaling Technology, Tokyo, Japan). The signals were detected using chemiluminescence.

2.6. Cardiac and plasma UA measurement

Cardiac tissue UA content and plasma UA level were measured at day 7 using a UA assay kit (Sigma) according to the manufacturer's protocol. The heart tissue was homogenized in assay buffer and centrifuged (13,000 g, 10 min, 4 °C). The blood was drawn immediately after the heart excision and centrifuged (3000 g, 10 min, 4 °C) to collect plasma. The resulting supernatant extracted from the tissue homogenate or plasma was mixed with assay buffer containing a UA probe and enzyme mix at 37 °C for 30 min, protected from light. After incubation, the absorbance was measured at 570 nm. Tissue cardiac UA concentration was corrected based on the protein concentration of the supernatant measured by the Bradford protein assay.

2.7. Cardiac nitrite and nitrate measurement

The mouse hearts at day 7 after Dox administration were washed for 2–3 min by Langendorff apparatus to remove blood cells and frozen in the liquid nitrogen. The frozen heart tissue was homogenized in T-PER Tissue Protein Extraction followed by centrifugation (14,000 g, 10 min, 4 °C). The supernatant of heart tissue homogenate was centrifuged (14,000 g, 30 min, 4 °C) through a 10 kDa molecular mass cut-off filter (Amicon, Millipore Corporation, Bedford, MA, USA) to remove substances larger than 10 kDa. The filtrates were analyzed by using a Nitrite/Nitrate Assay kit (NK05, Dojindo, Japan) according to manufactured protocol. For measuring nitrite concentration, Griess Reagent A was added to the ultrafiltrate and incubated at room temperature for 5 min. Then, Griess Regent B was added to the mixture and incubated at room temperature for 10 min. The tissue nitrite concentration was measured with a microplate reader at the absorbance of 540 nm [37]. For measuring nitrate-plus-nitrite concentration, the ultrafiltrate was mixed with the Nitrate Reductase solution and the Enzyme Co-factors solution, and incubated at room temperature for 2 h, followed by the same protocol of nitrite measurement described above. Nitrate concentration was obtained by subtracting nitrite concentration from nitrate-plus-nitrite concentration. The nitrite and nitrate concentrations were corrected by the protein concentration of the supernatant before ultrafiltration measured by a Bradford assay.

2.8. DAF-FM DA-derived fluorescence detection in the heart

The fluorescent probe (DAF-FM DA, GORYO chemical, Japan) was used to measure nitric oxide (NO) production in heart tissue homogenates as previously described [38]. The mice hearts at day 7 after Dox administration were washed for 2–3 min by Langendorff apparatus to remove blood cells and frozen in the liquid nitrogen. The frozen heart tissue was homogenized in 250 mM sucrose and 10 mM Tris-HCl (pH7.4), and centrifuged (500 g, 10min, 4 °C). The supernatant was incubated with 500 μM NAD^+, 500 μM NADH and 1 mM NADPH using PBS as a buffer. One hundred fifty μl of the mixed supernatants were transferred in triplicates to black microplates and DAF-FM DA (10 μM) was added to each well. Fluorescence readings were made at Ex/Em = 540/590 nm and measured every 60min for 10 h at 37 °C. The average fluorescence per hour was calculated as NO concentration.

2.9. Metabolite extraction

Mouse hearts at day 7 were washed in PBS (FUJIFILM, Wako Pure Chemical Corporation) at 4 °C, snap-frozen in liquid nitrogen, and stored at −80 °C prior to analyses. Approximately 30 mg of frozen tissue was plunged into 450–600 μL of 50% acetonitrile/MilliQ water containing internal standards (H3304-1002; Human Metabolome technologies [HMT], Inc., Tsuruoka, Japan) at 0 °C in order to inactivate enzymes. The tissue was homogenized thrice at 1500 rpm for 2 min using a tissue homogenizer, and then the homogenate was centrifuged at 2300 g and 4 °C for 5 min. Subsequently, 400 μL of the upper aqueous layer was centrifugally filtered through a Millipore 5-kDa cut-off filter at 9100 g and 4 °C for 120 min to remove proteins. The filtrate was centrifugally concentrated and re-suspended in 50 μL of Milli Q water for the capillary electrophoresis (CE)-MS analysis.

2.10. Metabolome analyses

Metabolome analyses were conducted using the C-SCOPE software package of HMT using CE-time of flight mass spectrometry (CE-TOFMS) for the cation analysis and CE-tandem mass spectrometry (CE-MS/MS) for the anion analysis based on the methods previously described [39,40]. In brief, the CE-TOFMS analysis was conducted using an Aligent CE capillary electrophoresis system equipped with an Aligent 6210 time of flight mass spectrometer (Aligent Technologies, Waldbronn, Germany). The systems were controlled by the Aligent G2201AA ChemStation software program, version B.03.01, for CE (Aligent Technologies) and connected by a fused silica capillary (50-μm inner diameter. × 80-cm total length) with commercial electrophoresis buffer (H3301-1001 and I3302-1023 for cation and anion analyses, respectively; HMT, Inc.) as the electrolyte. The spectrometer was scanned from m/z 50 to 1000 [39]. Peaks were extracted using MasterHands automatic integration software program (Keio University, Tsuruoka Yamagata, Japan) [41] and MassHunter Quantitative Analysis software program, B.04.00 (Aligent Technologies), in order to obtain peak information, including m/z, peak area and migration time (MT). Signal peaks were annotated according to the HMT metabolite database based on their m/z values with the MT. The concentrations of metabolite were calculated by normalizing the peak area of each metabolite with respect to the area of the internal standard and using standard curves with three-point calibrations. A hierarchical cluster analysis (HCA) and principal component analysis (PCA) were performed using HMT Inc.'s proprietary software programs, PeakStat and SampleStat, respectively. The metabolic pathway of the detected metabolites was plotted using Vusualization and Analysis of Networks containing Experimental Data (VANTED) software program [42].

2.11. Statistical analyses

The data are presented as the mean ± standard error of the mean (SEM) of at least three independent experiments. Student's t-test was used to compare the means of normally distributed continuous variables. One-way analysis of variance (ANOVA) followed by Tukey's post-hoc test was used for evaluations of the cardiac XO activity, plasma UA concentrations, echocardiographic data (LVDd, and LVPWd), Langendorff data (left ventricular developed pressure [LVDP], rate pressure product [RPP], and negative dp/dt), immunoblots, and cardiac tissue metabolites concentrations. Nonparametric data of cardiac UA content, echocardiographic data (IVSd, EF, FS, and LVDs), and positive dp/dt were compared between groups using Mann-Whitney U test when two groups were compared or Kruskal Wallis test with Dunn's post-hoc test when more than two groups were compared. All statistical calculations were performed using GraphPad Prism 8. A value of $P < 0.05$ was considered to be significant.

3. Results

3.1. Effects of Dox on body weight and heart weight

The body weight was significantly decreased in Dox-treated mice, regardless of the treatment with XO-inhibitors (Fig. 1B). This was mainly due to a decrease in dietary intake observed in Dox-treated subjects (Supplementary Fig. S1). Correspondingly, the heart weight was also decreased in Dox-treated mice (Fig. 1C), while the lung weight was comparable between the groups (Fig. 1D), indicating that a single injection of Dox (10 mg/kg) did not induce pulmonary congestion at day 7 in the present study.

3.2. Effects of Dox administration on the cardiac tissue XO activity

We first measured the XO enzymatic activities in various tissues of male ICR mice by Amplex Red fluorescence assay using xanthine as a substrate in order to assess the tissue distribution of XO activity. Under basal conditions, the XO activity was high in the small intestine, kidney, and liver but relatively low in the heart (Fig. 2A), consistent with the findings of a previous study [8]. This fluorescence assay actually detects tissue H_2O_2 production levels induced by XO activation, namely, measuring tissue XO-derived ROS levels. We found that XO-derived H_2O_2 levels were significantly increased in Dox-treated heart, which was substantially reduced by the treatment with XO-inhibitors (Fig. 2B). Based on these findings, cardiac tissue XO activity was measured more directly by a recently developed highly sensitive assay with liquid chromatography-mass spectrometry (LC/MS) using stable isotope-labeled xanthine [33]. Cardiac XO activity was significantly increased in Dox-treated mice compared to vehicle-treated controls (4.21 ± 0.26 nmol/5 min/mg protein vs. 2.86 ± 0.15 nmol/5 min/mg protein, $P < 0.001$, Fig. 2C), which was consistent with the results obtained using Amplex Red assay (Fig. 2B). Of note, XO-inhibitors significantly reduced cardiac XO activity, even in the vehicle-treated subjects ([Feb] 1.9 ± 0.22 nmol/5 min/mg protein; [Topi] 1.28 ± 0.21 nmol/5 min/mg protein, $P < 0.05$, and $P < 0.001$ vs. Control, respectively), and more substantial reduction of XO activity was observed in the Dox-treated subjects ([Feb] 2.31 ± 0.18 nmol/5 min/mg protein; [Topi] 1.40 ± 0.15 nmol/5 min/mg protein, $P < 0.001$ vs. Dox alone, Fig. 2C). The protein expression of XO was comparable between Dox-treated and control hearts (Fig. 2D). Furthermore, cardiac UA content was significantly increased in Dox-treated mice compared to vehicle-treated controls (5.31 ± 0.38 mg/g protein vs. 3.86 ± 0.22 mg/g protein, $P < 0.05$, Fig. 2E) and reduced by XO-inhibitors ([Feb] 2.30 ± 0.12 mg/g protein; [Topi] 1.86 ± 0.08 mg/g protein, $P < 0.01$ vs. Dox alone, Fig. 2E). Likewise, plasma UA level was significantly increased in Dox-treated mice compared to controls (4.45 ± 0.44 mg/dl vs. 3.27 ± 0.22 mg/dl, $P < 0.05$, Fig. 2F) and reduced by XO-inhibitors although the difference between Feb and Dox alone was not significant ([Feb] 3.29 ± 0.23 mg/dl; [Topi] 2.69 ± 0.33 mg/dl, $P = 0.053$, and $P < 0.01$ vs. Dox alone, respectively, Fig. 2F). XDH is an equivalent producer of UA and it needs

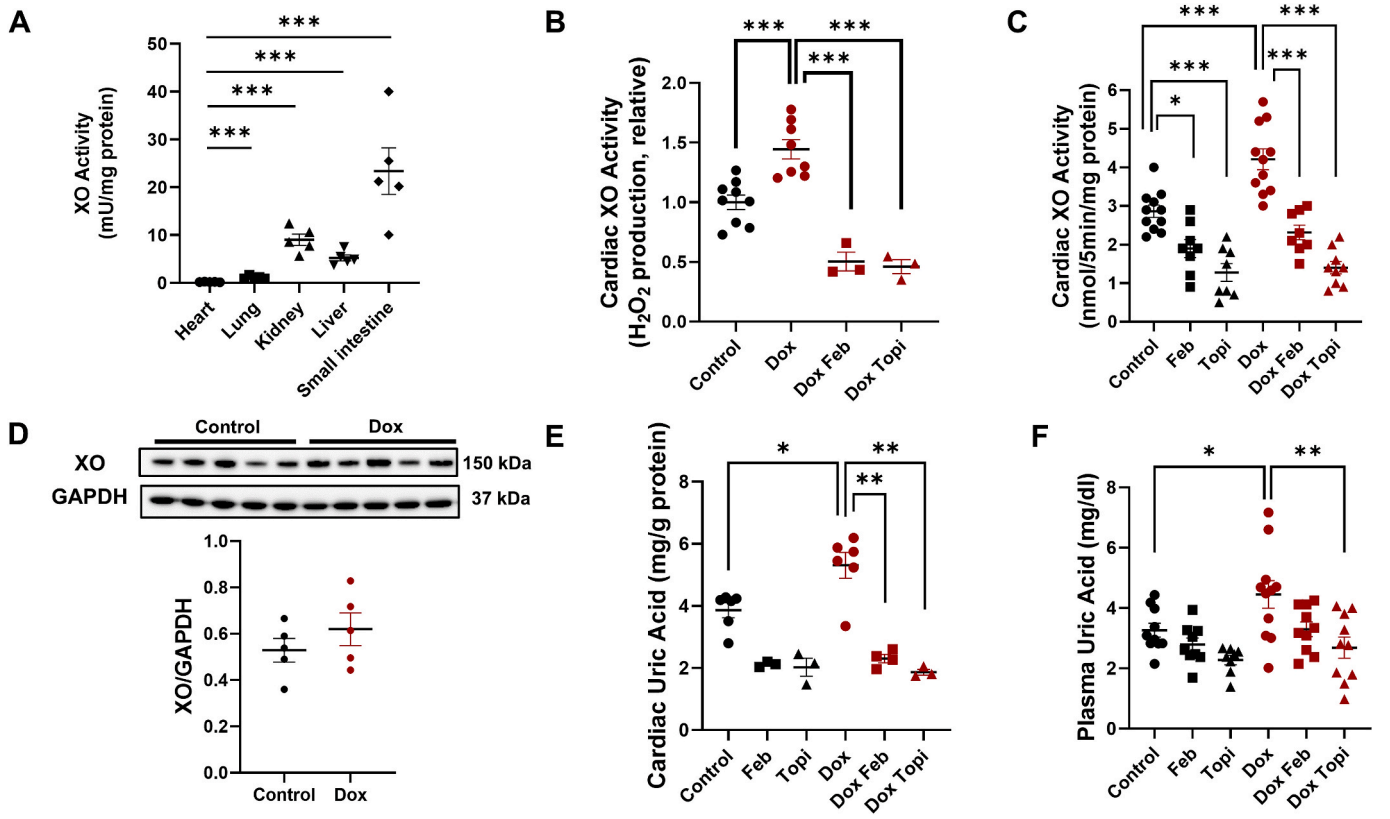

Fig. 2. The cardiac XO activity is increased in Dox-treated mice. (A) Various tissue XO activities measured by the Amplex Red assay (n = 5 each). (B) Cardiac XO activity (H2O2 production using xanthine as a substrate) normalized to vehicle-treated control at 7 days after Dox administration as measured by Amplex Red assay (Control, n = 9; Dox, n = 8; Dox + Feb, n = 3; Dox + Topi, n = 3). (C) The cardiac XO activity was increased at 7 days after Dox administration and reduced by XO-inhibitors, as measured by LC/MS (Control, n = 11; Feb, n = 8; Topi, n = 8; Dox, n = 11; Dox + Feb, n = 8; Dox + Topi, n = 9). (D) The protein expression of cardiac XO after vehicle or Dox administration (n = 5 each). The UA content in the heart (E) and plasma UA concentrations (F) were increased at 7 days after Dox administration ([Cardiac UA] Control, n = 6; Feb, n = 3; Topi, n = 3; Dox, n = 6; Dox + Feb, n = 4; Dox + Topi, n = 3; [Plasma UA] Control, n = 10; Feb, n = 9; Topi, n = 8; Dox, n = 11; Dox + Feb, n = 10; Dox + Topi, n = 10). Data are mean ± SEM. ***P < 0.001, **P < 0.01, and *P < 0.05 between indicated groups. (For interpretation of the references to colour in this figure legend, the reader is referred to the Web version of this article.)

to be considered. We found that cardiac tissue XDH activity was significantly increased in Dox-treated mice compared to vehicle-treated controls and XO-inhibitors significantly reduced cardiac XDH activity (Supplementary Fig. S2A). However, the ratio of XDH to XO in cardiac tissue was not markedly different between the groups, indicating that Dox treatment does not significantly affect the posttranslational conversion of XDH to XO in the cardiac tissue, at least in the present model (Supplementary Fig. S2B).

3.3. Effects of Dox administration and XO-inhibitors on the nitrate-nitrite-NO pathway in the heart

Recent studies have reported that XO is also a major nitrate to nitrite and nitrite to NO reductase, particularly under certain conditions, such as ischemia or conditions associated with compromised endothelial NO synthase (eNOS) [38,43]. We therefore also assessed the cardiac tissue levels of nitrate, nitrite, and NO (Supplementary Fig. S3). The levels of cardiac nitrate and nitrite were comparable between the groups (Supplementary Figs. S3A–S3B). The ratio of nitrite to nitrate, which indicates the activity of nitrate reduction to nitrite, tended to be higher in Dox-treated hearts than in vehicle-treated controls but not to a significant degree (0.340 ± 0.166 vs. 0.077 ± 0.029, P = 0.10), and XO-inhibitors did not significantly affect this ratio (Supplementary Fig. S3C). On the other hand, the cardiac tissue NO content was not increased in Dox-treated mice ([Dox] 32.3 ± 0.7 RFU/hour vs. [Control] 29.1 ± 1.5 RFU/hour, P = 0.16), but it was reduced by XO-inhibitors, although the difference between Topi and Dox alone was not significant ([Dox Feb] 25.8 ± 0.7 RFU/hour; [Dox Topi] 27.0 ± 1.6 RFU/hour, P < 0.05, and P = 0.09 vs. Dox alone, respectively, Supplementary Fig. S3D). These inconsistent data suggest that tissue XO activation in Dox-treated heart may influence the cardiac nitrate-nitrite-NO pathway, but its impact is not significant, at least in the present experimental model.

3.4. Effects of XO-inhibitors on Dox-induced cardiac dysfunction

To test the functional significance of the Dox-induced tissue XO activation in the heart, we assessed the cardiac function by echocardiography at day 6 (Fig. 3A–B and Online Videos) and by ex vivo Langendorff heart perfusion model at day 7 (Fig. 3C–E and Supplementary Fig. S4) after Dox administration.

LVEF and FS as assessed by echocardiography were markedly impaired in Dox-treated mice compared with vehicle-treated mice (Fig. 3A–B, Supplementary Table S1, and Online Videos). Treatment with either Feb or Topi resulted in a substantial improvement in both LVEF and FS. LVDs was significantly larger in Dox-treated mice than in vehicle-treated mice but significantly reduced after Topi treatment, and non-significant trend toward decrease after Feb treatment (P = 0.053), while LVDd was comparable between the groups.

To eliminate systemic influences from neurohumoral input as well as the effects of circulating hematopoietic cells, the cardiac function was also measured using an isolated Langendorff heart perfusion system [34–36]. Consistent with the echocardiographic data, LV developed pressure (LVDP), rate pressure product (RPP) (LVDP × heart rate, to

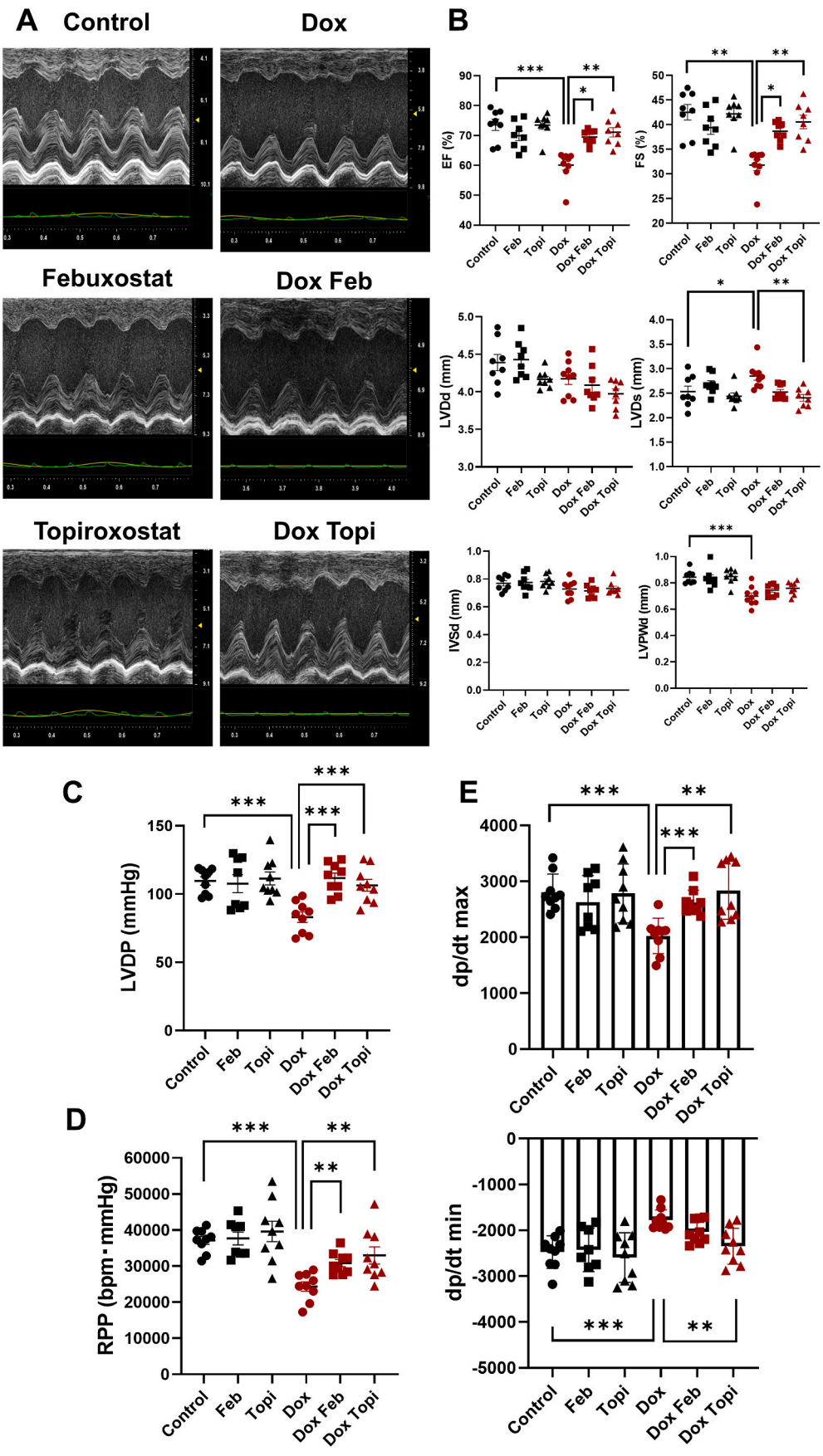

Fig. 3. XO-inhibitors attenuate Dox-induced cardiac dysfunction as assessed by echocardiography and ex vivo Langendorff heart perfusion model. (A) Representative M-mode echocardiograms obtained from vehicle- or Dox-treated mice with or without XO-inhibitors treatment. (B) XO-inhibitors improved cardiac function at 6 days after Dox administration, as indicated by EF and FS (Control, n = 8; Feb, n = 8; Topi, n = 8; Dox, n = 9; Dox + Feb, n = 8; Dox + Topi, n = 8). LVDP (C), RPP (D), positive and negative dp/dt (E) in vehicle- and Dox-treated mice hearts with or without XO-inhibitors treatment as assessed by ex vivo heart perfusion (Control, n = 9; Feb, n = 8; Topi, n = 9; Dox, n = 9; Dox + Feb, n = 9; Dox + Topi, n = 9). Data are mean ± SEM. ***P < 0.001, **P < 0.01, and *P < 0.05 between indicated groups.

assess the impact of the heart rate on the cardiac function), maximum rate of contraction/relaxation (±dp/dt), and coronary flow as assessed by ex vivo Langendorff heart perfusion were markedly impaired in Dox-treated mice compared to vehicle-treated mice (Fig. 3C–E, Supplementary Table S2 and Fig. S4). Treatment with either Feb or Topi resulted in a substantial improvement in all of these hemodynamic parameters.

3.5. Roles of apoptosis and ferroptosis in the effects of XO-inhibitors on Dox-induced cardiotoxicity

We next examined the possible involvement of the apoptotic pathway in the present model and found that Dox consistently induced apoptosis in the heart, as indicated by an increase in cleaved-caspase 3 and Bax levels and a decrease in Bcl-2 levels (Fig. 4A). Feb decreased the cleaved-caspase 3 levels and increased the Bcl-2 levels, while Topi decreased the Bax levels and tended to increase Bcl-2 levels (P = 0.08), suggesting that XO-inhibitors have anti-apoptotic effects with some variations.

A recent study indicated that ferroptosis plays an important role in Dox-induced cardiotoxicity [31]. Glutathione peroxidase 4 (GPX4) is an important antioxidant enzyme, and the disturbance of the GPX4-mediated redox balance is one of the defining characteristics of ferroptosis [44,45]. Thus, we also examined the expression of GPX-4 in the heart after Dox administration. GPX4 expression was significantly decreased in Dox-treated hearts but ameliorated by XO-inhibitors (Fig. 4B), indicating that anti-ferroptotic effects of XO-inhibitors might be partly involved in the present model of Dox-induced cardiotoxicity.

3.6. Cardiac metabolomes after Dox administration with or without XO-inhibitors treatment

We next measured the metabolites in the hearts in order to examine the effects of Dox on purine metabolism (Fig. 5 and Supplementary Fig. S5). Adenosine triphosphate (ATP), the ratio of ATP to adenosine diphosphate (ADP), and the adenylate energy charge tended to be decreased in Dox-treated mice but attenuated by XO-inhibitors, although the differences did not reach statistical significance due to the low number of subjects (Fig. 5 and Supplementary Figs. S5D–E). These data indicate that cellular energy metabolism is inhibited in the Dox-treated heart, and XO-inhibitors recover this inhibition. On the other hand, the major substrates in the pentose phosphate pathway (PPP), such as xyrulose-5-phosphate, ribose-5 phosphate, and ribose 1-phosphate, tended to be increased in Dox-treated mice but reduced by XO-inhibitors. Furthermore, the ratio of glucose 6- phosphate (G6P) to ribose 5-phosphate (R5P) trended lower in Dox-treated mice than in vehicle-treated mice, and XO inhibitors tended to increase this ratio (Supplementary Fig. S5F). These results indicate that PPP might be upregulated in Dox-treated hearts and inhibited by XO-inhibitors.

Metabolites from ATP degradation and PPP are ultimately converted to hypoxanthine, xanthine, and UA. Indeed, the hypoxanthine level in Dox-treated mice treated with XO-inhibitors was significantly higher than that in Dox-treated mice without XO inhibition, reflecting the fact that XO-inhibitors inhibit the conversion from hypoxanthine to xanthine and xanthine to UA in the heart. Accordingly, the cardiac UA level was non-significantly increased in Dox-treated mice but significantly decreased by XO-inhibitors, which was consistent with the findings of the direct measurement of UA content, shown in Fig. 2E.

Glycolysis in Dox-treated hearts tended to be impaired compared to vehicle-treated controls at the level of flux from fructose 6-phosphate (F6P) to fructose 1,6-diphosphate (F1,6P) (Supplementary Fig. S5J), which is the parameter of glycolysis in the heart [46]. Furthermore, the amounts of total tricarboxylic acid (TCA) cycle metabolites trended lower in Dox-treated hearts than in the controls (Supplementary Fig. S5K). Concomitantly, the levels of oxidized nicotinamide adenine dinucleotide (NADH), which is mainly generated from glycolysis and

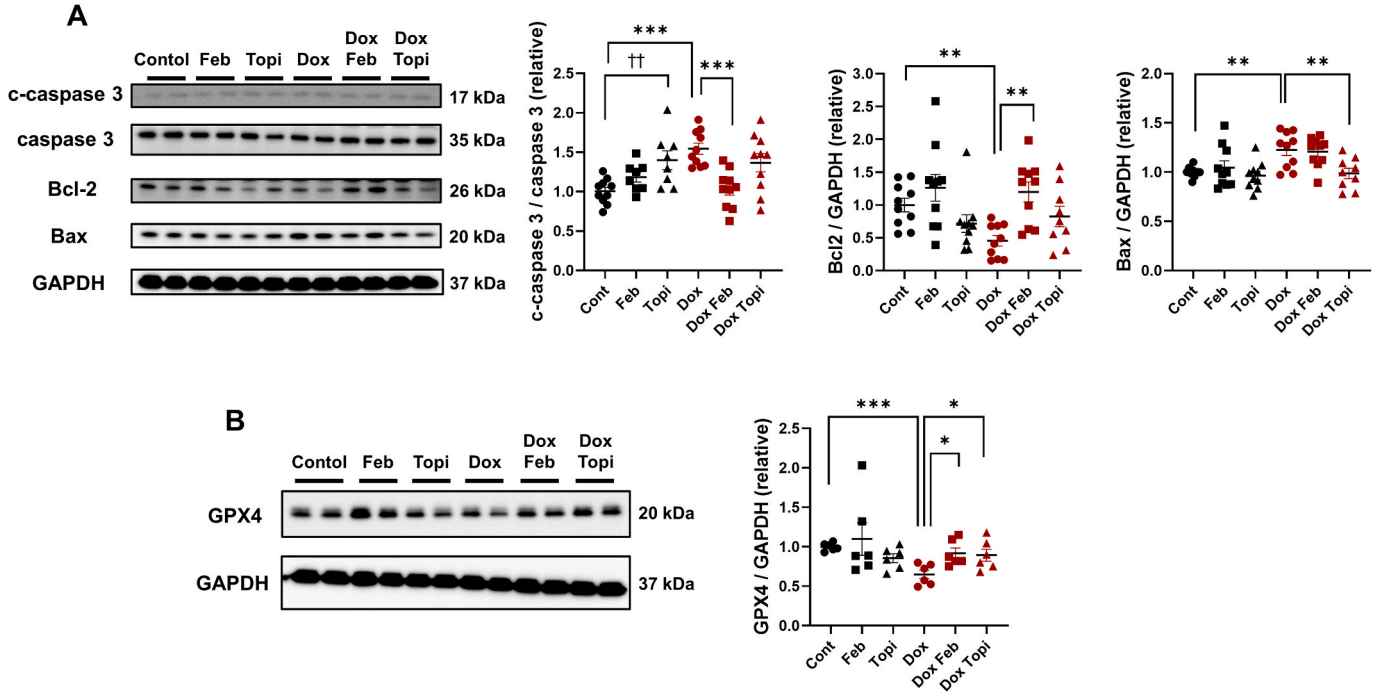

Fig. 4. Dox-induced apoptosis and ferroptosis in the heart are ameliorated by XO-inhibitors. (A) Representative immunoblots of the indicated apoptosis markers from cardiac lysates at 2 days after Dox administration with or without XO-inhibitor treatment are shown. ([c-caspase3] Control, n = 10; Feb, n = 8; Topi, n = 8; Dox, n = 10; Dox + Feb, n = 10; Dox + Topi, n = 10; [Bax] and [Bcl-2] Control, n = 10; Feb, n = 10; Topi, n = 10; Dox, n = 10; Dox + Feb, n = 10; Dox + Topi, n = 9). (B) Representative immunoblots of GPX4 from cardiac lysates at 2 days after Dox administration with or without XO-inhibitors treatment are shown (n = 6 each). GAPDH immunoblotting is shown as a loading control. Dot-whisker plots indicate densitometric quantitation normalized to vehicle-treated control without XO-inhibitors treatment. Data are mean ± SEM. ***P < 0.001, **P < 0.01, *P < 0.05, and ††P < 0.01 between indicated groups.

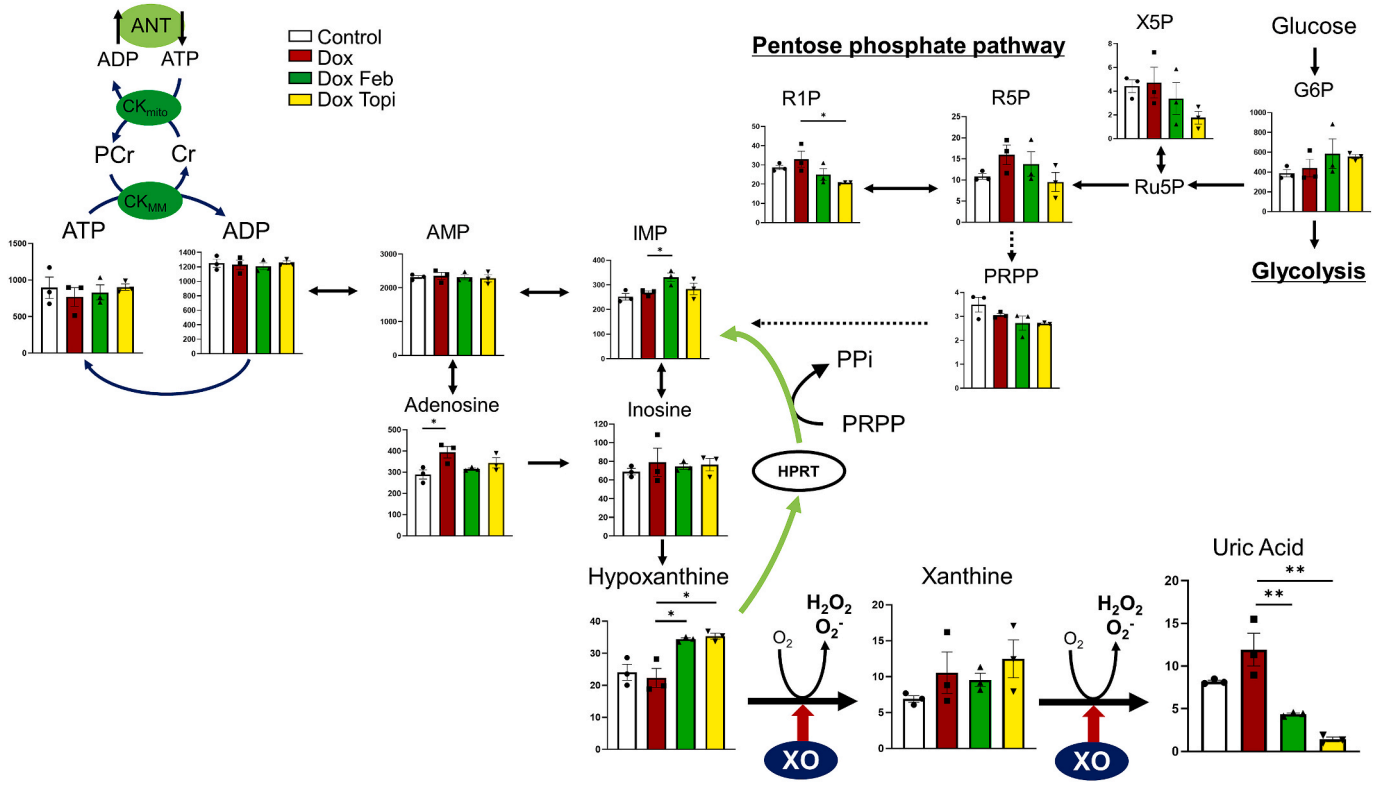

Fig. 5. Summary of changes in the cardiac tissue metabolomic profile as a function of Dox administration with or without XO-inhibitors treatment. The cardiac tissue metabolite concentrations in the purine metabolism pathway and pentose phosphate pathway at 7 days after Dox administration with or without XO-inhibitors treatment are shown (n = 3 each). Data are mean ± SEM. **P < 0.01 and *P < 0.05 between indicated groups. AMP, adenosine monophosphate, ANT, adenine nucleotide translocator; CK, creatine kinase; GDP, guanosine diphosphate; GMP, guanosine monophosphate; GTP, guanosine triphosphate; H_2O_2, hydrogen peroxide; HPRT, hypoxanthine guanine phosphoribosyltransferase; IMP, inosine monophosphate; MM, myocardial myofibril; Mito, mitochondria; O_2^-, superoxide anion; PPi, phosphoribosyl pyrophosphate; PRPP, phosphoribosyl diphosphate; R1P, ribose 1-phosphate; Ru5P, ribulose 5-phosphate; X5P, xylulose 5-phosphate; XMP, xanthosine monophosphate.

TCA cycle, as well as the NADH/NAD^+ ratio tended to be decreased in Dox-treated hearts (Supplementary Figs. S5A–C). These results indicate that Dox impairs glycolysis, TCA cycle, and ATP synthesis in the heart with the concomitant upregulation of PPP, leading to enhanced purine metabolism through XO activation. XO-inhibitors subsequently block the serial metabolic reaction of hypoxanthine–xanthine–UA, which may ultimately result in preserving the cardiac tissue ATP levels by inhibiting its degradation, in addition to exerting their antioxidative effects shown in Fig. 2B (Graphical Abstract).

4. Discussion

The major findings of the present study are that Dox induces cardiac tissue XO activation and increases the UA content, which is associated with an impaired LV function. Treatment with XO-inhibitors substantially reduces cardiac tissue XO activity and decreases UA content, leading to a significant improvement in the LV function in the Dox-treated heart. The potential underlying mechanisms are as follows: (1) XO-inhibitors substantially reduced XO-derived H_2O_2 production with concomitant downregulation of apoptotic and ferroptotic signaling pathways in the Dox-treated heart; and (2) XO-inhibitors conserve the cardiac tissue energy metabolism associated with modulation of the purine metabolic pathway.

In the present study using a recently developed highly sensitive assay with LC/MS [33], we clearly detected the tissue XO activity in the heart, although it was not very high compared to the activity in other organs, such as small intestine and liver. It is thus surprising that XO-inhibitors significantly improved the cardiac function by suppressing even a slight increase in the cardiac tissue XO activity induced by Dox administration. These findings suggest the following interpretations concerning tissue XO activation in the heart: First, the degree of tissue XO activation in the heart is likely to be more variable than that in other organs. Second, local tissue XO activation may play a less significant role in damage to other organs than in cardiac damage. In the heart, even a small increase in XO activation may directly induce significant myocardial damage. Therefore, the effects of XO-inhibitors on local tissue damage are likely to be more prominent in the heart than in other organs due to the naturally low XO activity. In other words, XO-inhibitors may exert a more significant and substantial impact on the heart than on other organs. Indeed, increasing evidence from both experimental [15,16,19,21–24,26,47] and clinical [25,48–50] studies suggests a critical role for XO-inhibitors in various models of heart failure, despite inconsistent findings concerning the cardiac XO activation levels.

XDH is an equivalent producer of UA, and cardiac XDH activity showed a similar trend to cardiac XO activity in the present study (Supplementary Fig. S2A). The XDH/XO ratio is reported to be approximately 5–7 in vivo [11,12], which is consistent with the present findings, suggesting that the present data on XDH and XO activities measured by LC/MS accurately reflect the in vivo physiological XOR kinetics. Given that Dox treatment did not facilitate the conversion between XDH and XO (Supplementary Fig. S2B) or NADH production (Supplementary Fig. S5A) but did increase the tissue H_2O_2 levels (Fig. 2B), the Dox-induced cardiotoxicity observed in the present study is most likely due to tissue XO activation per se rather than XDH activation. Meanwhile, XO concomitantly produces superoxide anion, which is also produced by NADH/NADPH oxidase and uncoupled eNOS [51]. Further studies are therefore warranted to determine whether or not tissue superoxide anion is increased in the present Dox-induced

cardiotoxicity model and to fully delineate the role of XO activation as well as the other two enzymes.

While XO is generally recognized as a source of ROS, XOR has been suggested to mediate NO formation via the reduction of nitrate and nitrite, conferring cardioprotection in various cardiovascular diseases [38,43,52]. However, the results of the present study investigating XOR-dependent activation of nitrate-nitrite-NO pathway in Dox-treated heart were inconsistent and didn't show significant differences between the groups (Supplementary Figs. S3C–D). Taken together with the negative findings on a switch of XOR formation as described above, the nitrate-nitrite-NO pathway might be partly involved in the current Dox-induced cardiotoxicity model, albeit without a substantial impact. As this pathway has been shown to act as a compensatory mechanism under conditions in which the eNOS activity is compromised [38], and given reports that Dox induces endothelial damage in the heart [53], further research is warranted to explore the pathophysiological significance of the nitrate-nitrite-NO pathway in Dox-induced cardiotoxicity with different protocols.

We previously reported in a clinical study that a high UA level is causally related to LV dysfunction and vice versa, suggesting that there is a possible cause-and-effect linkage between these factors [7]. Based on these clinical findings, the proposed mechanisms underlying the close linkage between the upregulation of the cardiac tissue XO activity and the corresponding increase in the cardiac tissue UA content and the impaired LV function in the Dox-treated heart is as follows (Graphical Abstract): ATP produced in the mitochondria is transferred to myofibrils through a creatine kinase energy shuttle (Cr-shuttle) and used by the contractile mechanism to form ADP [54]; under conditions of ATP dissipation and reduced Cr-shuttle, such as heart failure [55], the metabolic turnover of the purine metabolism is increased, and the breakdown paths below ADP are activated, eventually reaching the breakdown endpoint of UA via XO activation [17,54]. With this mechanism, the elevated tissue UA levels in the Dox-treated hearts are likely to be due to upregulated cardiac XO activity, which induces oxidative stress [56], leading to Cr-shuttle inhibition (vicious cycle formation) [54]. Likewise, the increased UA levels in both cardiac tissue and plasma (thought to be partly secreted from the failing heart [3]) of Dox-treated mice per se may also induce ROS generation. Inhibition of cardiac XO would thus in turn reduce cytosolic ROS, which enhances ATP formation via Cr-shuttle, thereby providing energy for contraction under conditions of Dox-induced LV dysfunction, as demonstrated in a recent study showing that XO-inhibitors accelerated Cr-shuttle [17]. Furthermore, the metabolome analyses in the present study indicated the accelerated above-described purine metabolism with concomitant enhanced PPP in Dox-treated hearts and showed that XO-inhibitors block the paths of ATP degradation. Likewise, hypoxanthine was accumulated in XO-inhibitors-treated hearts, and thus it is possible that XO-inhibitors facilitate the conversion from hypoxanthine to inosine monophosphate (IMP) by hypoxanthine phosphoribosyltransferase (HPRT), namely, purine salvage pathway, as previously reported in the heart and kidney [29,57,58]. Taken together, the present findings suggest that XO-inhibitors ameliorate Dox-induced cardiac dysfunction by conserving the cardiac tissue ATP content via accelerating ATP supply and reducing ATP degradation pathway.

The previous studies by Radi and Parks et al. demonstrated the antioxidant role of UA by inhibiting XO at physiological levels in plasma [10,59]. It is possible that this negative feedback also occurred in the present study model, although UA plays opposite roles between organ tissue and plasma, functioning as a pro-oxidant in the intracellular environment but an anti-oxidant in the extracellular environment. Based on the present findings that the cardiac tissue XO activity and UA content levels changed in parallel (observed both in direct measurements [Fig. 2E] and metabolome analyses [Fig. 5]), it is unlikely that UA inhibits XO in the heart of the present model. Meanwhile, it is also possible that XO activation by Dox-treatment may overwhelm UA-mediated XO inhibition. Further studies using other anti-hyperuricemic agents, such as urate reabsorption inhibitors, will help elucidate the direct effects of UA levels on the tissue XO activity.

Only a limited number of studies have shown the potential role of XO activation in Dox-induced cardiotoxicity [47]. Although the major mechanism for Dox-induced cardiotoxicity remains controversial, ROS plays a critical role at any rate [27–29,60], and in fact, the present study suggests that XO-derived H_2O_2 production is significantly involved (Fig. 2B). Likewise, increasing evidence indicates that increased ferroptosis [31], which is programmed iron-dependent cell death [44], as well as mitochondrial iron accumulation [30] are also deeply involved. We found that GPX4 expression, a negative regulator of ferroptosis [45], was decreased in Dox-treated hearts but improved by XO-inhibitors, indicating that XO-inhibitors attenuate Dox-induced ferroptosis in the heart, although the precise mechanisms by which cardiac XO upregulates the ferroptotic pathway remain unknown. We also found that the apoptotic pathway is upregulated in Dox-treated hearts by investigating the expression of cleaved-caspase 3, Bcl-2, and Bax, consistent with a series of previous studies [47], and attenuated by XO-inhibitors with some variations. XO-inhibitors thus attenuate Dox-induced cardiotoxicity by suppressing various cell-death pathways, presumably through the antioxidative effects. Further studies are also warranted to fully delineate the mechanisms by which Dox induces tissue XO activation in the heart.

Several limitations associated with the present study warrant mention. First, we examined a model of acute Dox-induced cardiac dysfunction, so the pathogenesis and changes in the energy metabolism might differ from those in chronic Dox-treated models (that actually have a higher mortality with concomitant serious peritonitis during experimental protocol by our hand). Second, given that XO is also expressed and activated in endothelial cells, future studies should investigate the effects of XO-inhibitors on Dox-induced myocardial injury in vitro cardiomyocytes, although a considerable number of cells will be required to measure the myocardial XO activity using the highly sensitive LC/MS assay. Third, a multidirectional approach is required for the assessment of ferroptosis, although a definitive methodology for the detection of ferroptosis has not yet been established. Finally, the sample size in the metabolome analysis was too small to determine statistical significance between groups. Future investigations should directly measure the metabolites of interest as well as the enzymatic activity that catalyzes the reaction.

5. Conclusion

Our data demonstrate that the tissue XO activity as well as UA content are increased in the Dox-treated heart, which is associated with an impaired cardiac function. XO-inhibitors reduce the cardiac tissue XO activity and UA content and improve cardiac function in the Dox-treated heart. These findings are partly explained by the inhibition of XO-derived oxidative stress and cell death signals as well as the maintenance of cardiac energy metabolism associated with modulation of the purine metabolic pathway in the subjects treated with XO-inhibitors. The present study suggests that pharmacological XO inhibition represents a potential therapeutic strategy for the treatment of Dox-induced cardiotoxicity.

Declaration of competing interest

None declared. Outside this study, Michihiro Yoshimura reports personal fees from Mochida Pharmaceutical Co., Ltd., personal fees from Daiichi Sankyo Co., Ltd., personal fees from Pfizer Japan Inc., personal fees from Kowa Co., Ltd., grants and personal fees from Mitsubishi Tanabe Pharma Corporation, grants form Teijin Pharma Ltd., grants from Astellas Pharma Inc., grants from Shionogi & Co., Ltd.

Acknowledgments

The authors are grateful to Mr. Naoki Ashizawa, Ms. Chiharu Hagihara, Mr. Keisuke Motoki, Mr. Koji Matsumoto and Mr. Takashi Iwanaga (Research Laboratories 2, Fuji Yakuhin Co.) for their excellent technical support in measuring the cardiac tissue XO activity with LC/MS assay. The authors are also grateful to Dr. Toru Akaike and Prof. Susumu Minamisawa (Department of Cell Physiology, The Jikei University of Medicine) for their excellent support in using Vevo 3100 system.

Appendix A. Supplementary data

Supplementary data to this article can be found online at https://doi.org/10.1016/j.freeradbiomed.2020.10.303.

Funding

This work was supported in part by grants-in-aid for the Ministry of Education Culture, Sports, Science and Technology [JP17K09531], [JP20K08435] (to T. Nagoshi) and [JP19K08592] (to M. Yoshimura).

References

[1] S. Masi, N.R. Pugliese, S. Taddei, The difficult relationship between uric acid and cardiovascular disease, Eur. Heart J. 40 (36) (2019) 3055–3057, https://doi.org/10.1093/eurheartj/ehz166.

[2] S.D. Anker, W. Doehner, M. Rauchhaus, R. Sharma, D. Francis, C. Knosalla, C. H. Davos, M. Cicoira, W. Shamim, M. Kemp, R. Segal, K.J. Osterziel, F. Leyva, R. Hetzer, P. Ponikowski, A.J. Coats, Uric acid and survival in chronic heart failure: validation and application in metabolic, functional, and hemodynamic staging, Circulation 107 (15) (2003) 1991–1997, https://doi.org/10.1161/01.CIR.0000065637.10517.A0.

[3] H. Sakai, T. Tsutamoto, T. Tsutsui, T. Tanaka, C. Ishikawa, M. Horie, Serum level of uric acid, partly secreted from the failing heart, is a prognostic marker in patients with congestive heart failure, Circ. J. 70 (8) (2006) 1006–1011, https://doi.org/10.1253/circj.70.1006.

[4] D. Toyoki, S. Shibata, E. Kuribayashi-Okuma, N. Xu, K. Ishizawa, M. Hosoyamada, S. Uchida, Insulin stimulates uric acid reabsorption via regulating urate transporter 1 and ATP-binding cassette subfamily G member 2, Am. J. Physiol. Ren. Physiol. 313 (3) (2017) F826–F834, https://doi.org/10.1152/ajprenal.00012.2017.

[5] S. Hamaguchi, T. Furumoto, M. Tsuchihashi-Makaya, K. Goto, D. Goto, T. Yokota, S. Kinugawa, H. Yokoshiki, A. Takeshita, H. Tsutsui, J.-C. Investigators, Hyperuricemia predicts adverse outcomes in patients with heart failure, Int. J. Cardiol. 151 (2) (2011) 143–147, https://doi.org/10.1016/j.ijcard.2010.05.002.

[6] H. Huang, B. Huang, Y. Li, Y. Huang, J. Li, H. Yao, X. Jing, J. Chen, J. Wang, Uric acid and risk of heart failure: a systematic review and meta-analysis, Eur. J. Heart Fail. 16 (1) (2014) 15–24, https://doi.org/10.1093/eurjhf/hft132.

[7] Y. Tanaka, T. Nagoshi, M. Kawai, G. Uno, S. Ito, A. Yoshii, H. Kimura, Y. Inoue, K. Ogawa, T.D. Tanaka, K. Minai, T. Ogawa, M. Yoshimura, Close linkage between serum uric acid and cardiac dysfunction in patients with ischemic heart disease according to covariance structure analysis, Sci. Rep. 7 (1) (2017) 2519, https://doi.org/10.1038/s41598-017-02707-y.

[8] Y. Tsushima, H. Nishizawa, Y. Tochino, H. Nakatsuji, R. Sekimoto, H. Nagao, T. Shirakura, K. Kato, K. Imaizumi, H. Takahashi, M. Tamura, N. Maeda, T. Funahashi, I. Shimomura, Uric acid secretion from adipose tissue and its increase in obesity, J. Biol. Chem. 288 (38) (2013) 27138–27149, https://doi.org/10.1074/jbc.M113.485094.

[9] T. Nishino, K. Okamoto, Y. Kawaguchi, H. Hori, T. Matsumura, B.T. Eger, E.F. Pai, T. Nishino, Mechanism of the conversion of xanthine dehydrogenase to xanthine oxidase: identification of the two cysteine disulfide bonds and crystal structure of a non-convertible rat liver xanthine dehydrogenase mutant, J. Biol. Chem. 280 (26) (2005) 24888–24894, https://doi.org/10.1074/jbc.M501830200.

[10] S. Tan, R. Radi, F. Gaudier, R.A. Evans, A. Rivera, K.A. Kirk, D.A. Parks, Physiologic levels of uric acid inhibit xanthine oxidase in human plasma, Pediatr. Res. 34 (3) (1993) 303–307, https://doi.org/10.1203/00006450-199309000-00013.

[11] S.L. Thompson-Gorman, J.L. Zweier, Evaluation of the role of xanthine oxidase in myocardial reperfusion injury, J. Biol. Chem. 265 (12) (1990) 6656–6663.

[12] T. Kusano, D. Ehirchiou, T. Matsumura, V. Chobaz, S. Nasi, M. Castelblanco, A. So, C. Lavanchy, H. Acha-Orbea, T. Nishino, K. Okamoto, N. Busso, Targeted knock-in mice expressing the oxidase-fixed form of xanthine oxidoreductase favor tumor growth, Nat. Commun. 10 (1) (2019) 4904, https://doi.org/10.1038/s41467-019-12565-z.

[13] R. Harrison, Structure and function of xanthine oxidoreductase: where are we now? Free Radic. Biol. Med. 33 (6) (2002) 774–797, https://doi.org/10.1016/s0891-5849(02)00956-5.

[14] B. Butts, D.A. Calhoun, T.S. Denney Jr., S.G. Lloyd, H. Gupta, K.K. Gaddam, I. Aban, S. Oparil, P.W. Sanders, R. Patel, J.F. Collawn, L.J. Dell'Italia, Plasma xanthine oxidase activity is related to increased sodium and left ventricular hypertrophy in resistant hypertension, Free Radic. Biol. Med. 134 (2019) 343–349, https://doi.org/10.1016/j.freeradbiomed.2019.01.029.

[15] H. Omizo, Y. Tamura, C. Morimoto, M. Ueno, Y. Hayama, E. Kuribayashi-Okuma, S. Uchida, S. Shibata, Cardio-renal protective effect of the xanthine oxidase inhibitor febuxostat in the 5/6 nephrectomy model with hyperuricemia, Sci. Rep. 10 (1) (2020) 9326, https://doi.org/10.1038/s41598-020-65706-6.

[16] H. Nambu, S. Takada, S. Maekawa, J. Matsumoto, N. Kakutani, T. Furihata, R. Shirakawa, T. Katayama, T. Nakajima, K. Yamanashi, Y. Obata, I. Nakano, M. Tsuda, A. Saito, A. Fukushima, T. Yokota, J. Nio-Kobayashi, H. Yasui, K. Higashikawa, Y. Kuge, T. Anzai, H. Sabe, S. Kinugawa, Inhibition of xanthine oxidase in the acute phase of myocardial infarction prevents skeletal muscle abnormalities and exercise intolerance, Cardiovasc. Res. (2020), https://doi.org/10.1093/cvr/cvaa127 in press.

[17] G.A. Hirsch, P.A. Bottomley, G. Gerstenblith, R.G. Weiss, Allopurinol acutely increases adenosine triphospate energy delivery in failing human hearts, J. Am. Coll. Cardiol. 59 (9) (2012) 802–808, https://doi.org/10.1016/j.jacc.2011.10.895.

[18] G. Kamalov, R.A. Ahokas, W. Zhao, A.U. Shahbaz, S.K. Bhattacharya, Y. Sun, I. C. Gerling, K.T. Weber, Temporal responses to intrinsically coupled calcium and zinc dyshomeostasis in cardiac myocytes and mitochondria during aldosteronism, Am. J. Physiol. Heart Circ. Physiol. 298 (2) (2010) H385–H394, https://doi.org/10.1152/ajpheart.00593.2009.

[19] N. Engberding, S. Spiekermann, A. Schaefer, A. Heineke, A. Wiencke, M. Muller, M. Fuchs, D. Hilfiker-Kleiner, B. Hornig, H. Drexler, U. Landmesser, Allopurinol attenuates left ventricular remodeling and dysfunction after experimental myocardial infarction: a new action for an old drug? Circulation 110 (15) (2004) 2175–2179, https://doi.org/10.1161/01.CIR.0000144303.24894.1C.

[20] V. Mellin, M. Isabelle, A. Oudot, C. Vergely-Vandriesse, C. Monteil, B. Di Meglio, J. P. Henry, B. Dautreaux, L. Rochette, C. Thuillez, P. Mulder, Transient reduction in myocardial free oxygen radical levels is involved in the improved cardiac function and structure after long-term allopurinol treatment initiated in established chronic heart failure, Eur. Heart J. 26 (15) (2005) 1544–1550, https://doi.org/10.1093/eurheartj/ehi305.

[21] J.D. Gladden, B.R. Zelickson, C.C. Wei, E. Ulasova, J. Zheng, M.I. Ahmed, Y. Chen, M. Bamman, S. Ballinger, V. Darley-Usmar, L.J. Dell'Italia, Novel insights into interactions between mitochondria and xanthine oxidase in acute cardiac volume overload, Free Radic. Biol. Med. 51 (11) (2011) 1975–1984, https://doi.org/10.1016/j.freeradbiomed.2011.08.022.

[22] G. Jia, J. Habibi, B.P. Bostick, L. Ma, V.G. DeMarco, A.R. Aroor, M.R. Hayden, A. T. Whaley-Connell, J.R. Sowers, Uric acid promotes left ventricular diastolic dysfunction in mice fed a Western diet, Hypertension 65 (3) (2015) 531–539, https://doi.org/10.1161/HYPERTENSIONAHA.114.04737.

[23] A. Namai-Takahashi, A. Sakuyama, T. Nakamura, T. Miura, J. Takahashi, R. Kurosawa, M. Kohzuki, O. Ito, Xanthine oxidase inhibitor, febuxostat ameliorates the high salt intake-induced cardiac hypertrophy and fibrosis in dahl salt-sensitive rats, Am. J. Hypertens. 32 (1) (2019) 26–33, https://doi.org/10.1093/ajh/hpy143.

[24] Y. Kinugasa, K. Ogino, Y. Furuse, T. Shiomi, H. Tsutsui, T. Yamamoto, O. Igawa, I. Hisatome, C. Shigemasa, Allopurinol improves cardiac dysfunction after ischemia-reperfusion via reduction of oxidative stress in isolated perfused rat hearts, Circ. J. 67 (9) (2003) 781–787, https://doi.org/10.1253/circj.67.781.

[25] S. Baldus, K. Mullerleile, P. Chumley, D. Steven, V. Rudolph, G.K. Lund, H. J. Staude, A. Stork, R. Koster, J. Kahler, C. Weiss, T. Munzel, T. Meinertz, B. A. Freeman, T. Heitzer, Inhibition of xanthine oxidase improves myocardial contractility in patients with ischemic cardiomyopathy, Free Radic. Biol. Med. 41 (8) (2006) 1282–1288, https://doi.org/10.1016/j.freeradbiomed.2006.07.010.

[26] S. Tanno, K. Yamamoto, Y. Kurata, M. Adachi, Y. Inoue, N. Otani, M. Mishima, Y. Yamamoto, M. Kuwabara, K. Ogino, J. Miake, H. Ninomiya, Y. Shirayoshi, F. Okada, K. Yamamoto, I. Hisatome, Protective effects of topiroxostat on an ischemia-reperfusion model of rat hearts, Circ. J. 82 (4) (2018) 1101–1111, https://doi.org/10.1253/circj.CJ-17-1049.

[27] Y. Zhao, S. Miriyala, L. Miao, M. Mitov, D. Schnell, S.K. Dhar, J. Cai, J.B. Klein, R. Sultana, D.A. Butterfield, M. Vore, I. Batinic-Haberle, S. Bondada, D.K. St Clair, Redox proteomic identification of HNE-bound mitochondrial proteins in cardiac tissues reveals a systemic effect on energy metabolism after doxorubicin treatment, Free Radic. Biol. Med. 72 (2014) 55–65, https://doi.org/10.1016/j.freeradbiomed.2014.03.001.

[28] J.S. Koh, C.O. Yi, R.W. Heo, J.W. Ahn, J.R. Park, J.E. Lee, J.H. Kim, J.Y. Hwang, G. S. Roh, Protective effect of cilostazol against doxorubicin-induced cardiomyopathy in mice, Free Radic. Biol. Med. 89 (2015) 54–61, https://doi.org/10.1016/j.freeradbiomed.2015.07.016.

[29] P. Efentakis, A. Varela, E. Chavdoula, F. Sigala, D. Sanoudou, R. Tenta, K. Gioti, N. Kostomitsopoulos, A. Papapetropoulos, A. Tasouli, D. Farmakis, C.H. Davos, A. Klinakis, T. Suter, D.V. Cokkinos, E.K. Iliodromitis, P. Wenzel, I. Andreadou, Levosimendan prevents doxorubicin-induced cardiotoxicity in time- and dose-dependent manner: implications for inotropy, Cardiovasc. Res. 116 (3) (2020) 576–591, https://doi.org/10.1093/cvr/cvz163.

[30] Y. Ichikawa, M. Ghanefar, M. Bayeva, R. Wu, A. Khechaduri, S.V. Naga Prasad, R. K. Mutharasan, T.J. Naik, H. Ardehali, Cardiotoxicity of doxorubicin is mediated through mitochondrial iron accumulation, J. Clin. Invest. 124 (2) (2014) 617–630, https://doi.org/10.1172/JCI72931.

[31] X. Fang, H. Wang, D. Han, E. Xie, X. Yang, J. Wei, S. Gu, F. Gao, N. Zhu, X. Yin, Q. Cheng, P. Zhang, W. Dai, J. Chen, F. Yang, H.T. Yang, A. Linkermann, W. Gu, J. Min, F. Wang, Ferroptosis as a target for protection against cardiomyopathy, Proc. Natl. Acad. Sci. U. S. A. 116 (7) (2019) 2672–2680, https://doi.org/10.1073/pnas.1821022116.

[32] E. Yamamoto, K. Kataoka, T. Yamashita, Y. Tokutomi, Y.F. Dong, S. Matsuba, H. Ogawa, S. Kim-Mitsuyama, Role of xanthine oxidoreductase in the reversal of diastolic heart failure by candesartan in the salt-sensitive hypertensive rat, Hypertension 50 (4) (2007) 657–662, https://doi.org/10.1161/HYPERTENSIONAHA.107.095315.

[33] T. Murase, M. Nampei, M. Oka, N. Ashizawa, K. Matsumoto, A. Miyachi, T. Nakamura, Xanthine oxidoreductase activity assay in tissues using stable isotope-labeled substrate and liquid chromatography high-resolution mass spectrometry, J Chromatogr B Analyt Technol Biomed Life Sci 1008 (2016) 189–197, https://doi.org/10.1016/j.jchromb.2015.11.030.

[34] T. Nagoshi, T. Matsui, T. Aoyama, A. Leri, P. Anversa, L. Li, W. Ogawa, F. del Monte, J.K. Gwathmey, L. Grazette, B.A. Hemmings, D.A. Kass, H.C. Champion, A. Rosenzweig, PI3K rescues the detrimental effects of chronic Akt activation in the heart during ischemia/reperfusion injury, J. Clin. Invest. 115 (8) (2005) 2128–2138, https://doi.org/10.1172/JCI23073.

[35] Y. Kashiwagi, T. Nagoshi, T. Yoshino, T.D. Tanaka, K. Ito, T. Harada, H. Takahashi, M. Ikegami, R. Anzawa, M. Yoshimura, Expression of SGLT1 in human hearts and impairment of cardiac glucose uptake by phlorizin during ischemia-reperfusion injury in mice, PloS One 10 (6) (2015), e0130605, https://doi.org/10.1371/journal.pone.0130605.

[36] A. Yoshii, T. Nagoshi, Y. Kashiwagi, H. Kimura, Y. Tanaka, Y. Oi, K. Ito, T. Yoshino, T.D. Tanaka, M. Yoshimura, Cardiac ischemia-reperfusion injury under insulin-resistant conditions: SGLT1 but not SGLT2 plays a compensatory protective role in diet-induced obesity, Cardiovasc. Diabetol. 18 (1) (2019) 85, https://doi.org/10.1186/s12933-019-0889-y.

[37] K. Nakai, M.B. Kadiiska, J.J. Jiang, K. Stadler, R.P. Mason, Free radical production requires both inducible nitric oxide synthase and xanthine oxidase in LPS-treated skin, Proc. Natl. Acad. Sci. U. S. A. 103 (12) (2006) 4616–4621, https://doi.org/10.1073/pnas.0510352103.

[38] M. Peleli, C. Zollbrecht, M.F. Montenegro, M. Hezel, J. Zhong, E.G. Persson, R. Holmdahl, E. Weitzberg, J.O. Lundberg, M. Carlstrom, Enhanced XOR activity in eNOS-deficient mice: effects on the nitrate-nitrite-NO pathway and ROS homeostasis, Free Radic. Biol. Med. 99 (2016) 472–484, https://doi.org/10.1016/j.freeradbiomed.2016.09.004.

[39] Y. Ohashi, A. Hirayama, T. Ishikawa, S. Nakamura, K. Shimizu, Y. Ueno, M. Tomita, T. Soga, Depiction of metabolome changes in histidine-starved Escherichia coli by CE-TOFMS, Mol. Biosyst. 4 (2) (2008) 135–147, https://doi.org/10.1039/b714176a.

[40] T. Ooga, H. Sato, A. Nagashima, K. Sasaki, M. Tomita, T. Soga, Y. Ohashi, Metabolomic anatomy of an animal model revealing homeostatic imbalances in dyslipidaemia, Mol. Biosyst. 7 (4) (2011) 1217–1223, https://doi.org/10.1039/c0mb00141d.

[41] M. Sugimoto, D.T. Wong, A. Hirayama, T. Soga, M. Tomita, Capillary electrophoresis mass spectrometry-based saliva metabolomics identified oral, breast and pancreatic cancer-specific profiles, Metabolomics 6 (1) (2010) 78–95, https://doi.org/10.1007/s11306-009-0178-y.

[42] B.H. Junker, C. Klukas, F. Schreiber, VANTED: a system for advanced data analysis and visualization in the context of biological networks, BMC Bioinf. 7 (2006) 109, https://doi.org/10.1186/1471-2105-7-109.

[43] A. Webb, R. Bond, P. McLean, R. Uppal, N. Benjamin, A. Ahluwalia, Reduction of nitrite to nitric oxide during ischemia protects against myocardial ischemia-reperfusion damage, Proc. Natl. Acad. Sci. U. S. A. 101 (37) (2004) 13683–13688, https://doi.org/10.1073/pnas.0402927101.

[44] P.K. Mishra, A. Adameova, J.A. Hill, C.P. Baines, P.M. Kang, J.M. Downey, J. Narula, M. Takahashi, A. Abbate, H.C. Piristine, S. Kar, S. Su, J.K. Higa, N. K. Kawasaki, T. Matsui, Guidelines for evaluating myocardial cell death, Am. J. Physiol. Heart Circ. Physiol. 317 (5) (2019) H891–H922, https://doi.org/10.1152/ajpheart.00259.2019.

[45] F. Ursini, M. Maiorino, Lipid peroxidation and ferroptosis: the role of GSH and GPx4, Free Radic. Biol. Med. 152 (2020) 175–185, https://doi.org/10.1016/j.freeradbiomed.2020.02.027.

[46] H. Kouzu, T. Miki, M. Tanno, A. Kuno, T. Yano, T. Itoh, T. Sato, D. Sunaga, H. Murase, T. Tobisawa, M. Ogasawara, S. Ishikawa, T. Miura, Excessive degradation of adenine nucleotides by up-regulated AMP deaminase underlies afterload-induced diastolic dysfunction in the type 2 diabetic heart, J. Mol. Cell. Cardiol. 80 (2015) 136–145, https://doi.org/10.1016/j.yjmcc.2015.01.004.

[47] B. Krishnamurthy, N. Rani, S. Bharti, M. Golechha, J. Bhatia, T.C. Nag, R. Ray, S. Arava, D.S. Arya, Febuxostat ameliorates doxorubicin-induced cardiotoxicity in rats, Chem. Biol. Interact. 237 (2015) 96–103, https://doi.org/10.1016/j.cbi.2015.05.013.

[48] H.E. Cingolani, J.A. Plastino, E.M. Escudero, B. Mangal, J. Brown, N.G. Perez, The effect of xanthine oxidase inhibition upon ejection fraction in heart failure patients: La Plata Study, J. Card. Fail. 12 (7) (2006) 491–498, https://doi.org/10.1016/j.cardfail.2006.05.005.

[49] K. Ogino, M. Kato, Y. Furuse, Y. Kinugasa, K. Ishida, S. Osaki, T. Kinugawa, O. Igawa, I. Hisatome, C. Shigemasa, S.D. Anker, W. Doehner, Uric acid-lowering treatment with benzbromarone in patients with heart failure: a double-blind placebo-controlled crossover preliminary study, Circ Heart Fail 3 (1) (2010) 73–81, https://doi.org/10.1161/CIRCHEARTFAILURE.109.868604.

[50] Y. Otaki, T. Watanabe, D. Kinoshita, M. Yokoyama, T. Takahashi, T. Toshima, T. Sugai, T. Murase, T. Nakamura, S. Nishiyama, H. Takahashi, T. Arimoto, T. Shishido, T. Miyamoto, I. Kubota, Association of plasma xanthine oxidoreductase activity with severity and clinical outcome in patients with chronic heart failure, Int. J. Cardiol. 228 (2017) 151–157, https://doi.org/10.1016/j.ijcard.2016.11.077.

[51] H. Cai, D.G. Harrison, Endothelial dysfunction in cardiovascular diseases: the role of oxidant stress, Circ. Res. 87 (10) (2000) 840–844.

[52] J.O. Lundberg, M.T. Gladwin, A. Ahluwalia, N. Benjamin, N.S. Bryan, A. Butler, P. Cabrales, A. Fago, M. Feelisch, P.C. Ford, B.A. Freeman, M. Frenneaux, J. Friedman, M. Kelm, C.G. Kevil, D.B. Kim-Shapiro, A.V. Kozlov, J.R. Lancaster Jr., D.J. Lefer, K. McColl, K. McCurry, R.P. Patel, J. Petersson, T. Rassaf, V.P. Reutov, G.B. Richter-Addo, A. Schechter, S. Shiva, K. Tsuchiya, E.E. van Faassen, A. J. Webb, B.S. Zuckerbraun, J.L. Zweier, E. Weitzberg, Nitrate and nitrite in biology, nutrition and therapeutics, Nat. Chem. Biol. 5 (12) (2009) 865–869, https://doi.org/10.1038/nchembio.260.

[53] A.Z. Luu, B. Chowdhury, M. Al-Omran, H. Teoh, D.A. Hess, S. Verma, Role of endothelium in doxorubicin-induced cardiomyopathy, JACC Basic Transl Sci 3 (6) (2018) 861–870, https://doi.org/10.1016/j.jacbts.2018.06.005.

[54] L.H. Opie, Allopurinol for heart failure: novel mechanisms, J. Am. Coll. Cardiol. 59 (9) (2012) 809–812, https://doi.org/10.1016/j.jacc.2011.09.072.

[55] P.A. Bottomley, G.S. Panjrath, S. Lai, G.A. Hirsch, K. Wu, S.S. Najjar, A. Steinberg, G. Gerstenblith, R.G. Weiss, Metabolic rates of ATP transfer through creatine kinase (CK flux) predict clinical heart failure events and death, Sci. Transl. Med. 5 (215) (2013) 215re3, https://doi.org/10.1126/scitranslmed.3007328.

[56] W. Doehner, E.A. Jankowska, J. Springer, M. Lainscak, S.D. Anker, Uric acid and xanthine oxidase in heart failure - emerging data and therapeutic implications, Int. J. Cardiol. 213 (2016) 15–19, https://doi.org/10.1016/j.ijcard.2015.08.089.

[57] K. Fujii, A. Kubo, K. Miyashita, M. Sato, A. Hagiwara, H. Inoue, M. Ryuzaki, M. Tamaki, T. Hishiki, N. Hayakawa, Y. Kabe, H. Itoh, M. Suematsu, Xanthine oxidase inhibitor ameliorates postischemic renal injury in mice by promoting resynthesis of adenine nucleotides, JCI Insight 4 (22) (2019), https://doi.org/10.1172/jci.insight.124816.

[58] T. Tani, K. Okamoto, M. Fujiwara, A. Katayama, S. Tsuruoka, Metabolomics analysis elucidates unique influences on purine/pyrimidine metabolism by xanthine oxidoreductase inhibitors in a rat model of renal ischemia-reperfusion injury, Mol Med 25 (1) (2019) 40, https://doi.org/10.1186/s10020-019-0109-y.

[59] R. Radi, S. Tan, E. Prodanov, R.A. Evans, D.A. Parks, Inhibition of xanthine oxidase by uric acid and its influence on superoxide radical production, Biochim. Biophys. Acta 1122 (2) (1992) 178–182, https://doi.org/10.1016/0167-4838(92)90321-4.

[60] M.P. Cole, L. Chaiswing, T.D. Oberley, S.E. Edelmann, M.T. Piascik, S.M. Lin, K. K. Kiningham, D.K. St Clair, The protective roles of nitric oxide and superoxide dismutase in adriamycin-induced cardiotoxicity, Cardiovasc. Res. 69 (1) (2006) 186–197, https://doi.org/10.1016/j.cardiores.2005.07.012.